Robust Stability Analysis of the Simplified Virtual Synchronous Compensator for Grid Services and Grid Support

Robust Stability Analysis of the Simplified Virtual Synchronous Compensator for Grid Services and Grid Support

Vincenzo Mallemaci
Dipartimento Energia "Galileo Ferraris"
Politecnico di Torino
Torino, Italy
vincenzo.mallemaci@polito.it

Sante Pugliese
Chair of Power Electronics
Kiel University
Kiel, Germany
sapu@tf.uni-kiel.de

Fabio Mandrile
Dipartimento Energia "Galileo Ferraris"
Politecnico di Torino
Torino, Italy
fabio.mandrile@polito.it

Enrico Carpaneto
Dipartimento Energia "Galileo Ferraris"
Politecnico di Torino
Torino, Italy
enrico.carpaneto@polito.it

Radu Bojoi
Dipartimento Energia "Galileo Ferraris"
Politecnico di Torino
Torino, Italy
radu.bojoi@polito.it

Marco Liserre
Chair of Power Electronics
Kiel University
Kiel, Germany
ml@tf.uni-kiel.de

***Abstract*—Grid-connected converters that are controlled according to the Virtual Synchronous Machine (VSM) concept can provide ancillary services (e.g., the inertial behavior and the grid support during faults). The VSM is typically called VSG when it is in charge of processing the full power generation of the converter. The VSM can also operate as a Virtual Synchronous Compensator (VSC) when the virtual part only provides ancillary services and the conventional control structure of the converter is in charge of the power generation. This way, the VSC always operates at a very small load angle, showing higher damping and better transient stability with respect to a VSG. Independently of the operation mode (VSG or VSC), plant uncertainties such as wrong grid impedance estimation, grid reconfigurations and the influence of neighboring converters might affect the stability of grid-connected converters. Recent papers applied the μ-analysis to the VSG to study its robust stability for a given set of plant uncertainties. Nevertheless, the differences in terms of robustness between a VSC and a VSG have never been investigated in the literature. Therefore, this paper proposes a robust stability analysis applied to the Simplified Virtual Synchronous Compensator (S-VSC), a solution available in the literature that can operate as a virtual compensator or as a generator. The theoretical analysis demonstrates that a VSM working as VSC is more robust than the VSG mode operation. Moreover, this paper provides a method to experimentally validate the μ-analysis outcomes that confirm the theoretical results.**

***Index Terms*—robust stability, uncertainty, virtual synchronous machine, virtual synchronous compensator**

I. Introduction

Nowadays, conventional synchronous machines (SMs) guarantee grid frequency and voltage stability by providing ancillary services (e.g., inertial behavior, active and reactive power regulation, support during faults). However, the ongoing decommissioning of thermoelectric power plants (especially coal-based) will reduce the number of synchronous generators connected to the grid. Moreover, the power plants based on renewable energy sources (i.e., solar and wind) cannot inherently provide inertial support, as they are connected to the grid through static power electronic converters. The direct consequences are the reduction of the total power system inertia and the risk of compromising the grid frequency and voltage stability. Therefore, most recent grid codes require that even inverter-interfaced renewable energy sources must provide ancillary services [1]–[4]. The typical scheme under study consists of a three-phase inverter connected to the grid through an LCL filter, as depicted in Fig. 1. Control algorithms based on the Virtual Synchronous Machine (VSM) concept allow grid-connected converters to behave like conventional SMs, by providing grid services [5]–[7].

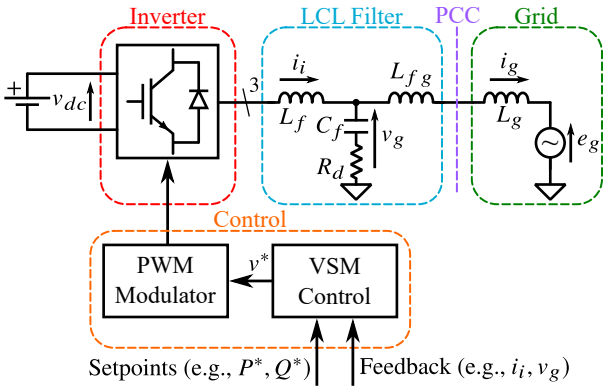

Fig. 1. Scheme of the system under study.

However, plant uncertainties (e.g., wrong grid impedance estimation), grid reconfigurations and the influence of neighboring converters might affect the stability of grid-connected converters. For this reason, recent papers investigated the robust stability of grid-connected converters for a given set of uncertainties, by applying the μ-analysis [8], [9]. In the

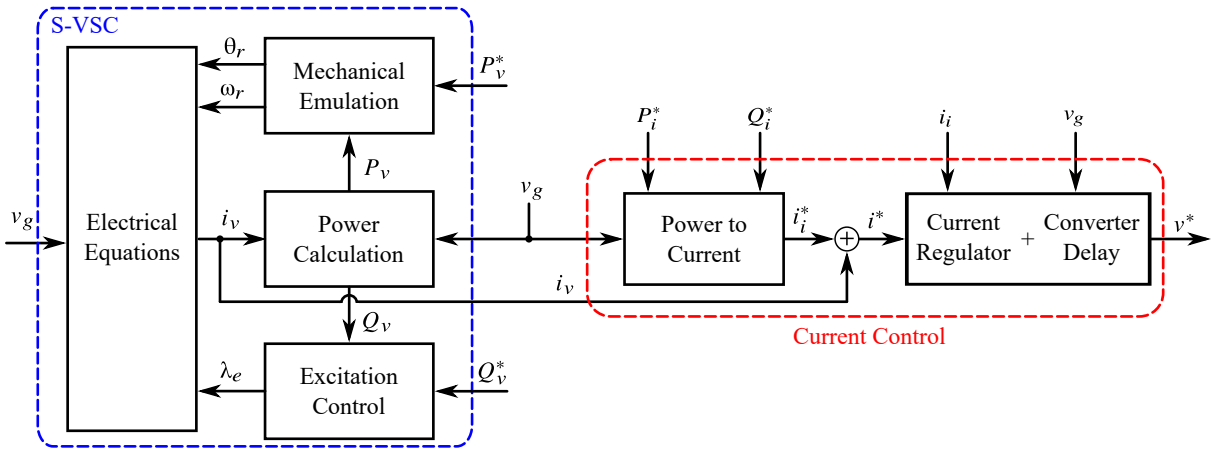

Fig. 2. Scheme of the grid-connected VSM control algorithm.

literature, this method has been applied to VSMs behaving as Virtual Synchronous Generators (VSGs). Nevertheless, a VSM can also operate as a Virtual Synchronous Compensator (VSC) [10] when the virtual model is in charge only of the grid services. The VSC always operates at a very small load angle, showing better performance in terms of transient stability and damping with respect to a VSG, as demonstrated in [10]. However, the differences in terms of robustness between a VSC and a VSG have never been investigated in the literature.

As a first contribution, this paper proposes the robust stability analysis of a VSM working both as a virtual compensator and generator. The proposed method has been applied to the Simplified Virtual Synchronous Compensator (S-VSC) [10] since the S-VSC can operate as both a VSC and a VSG. The theoretical results of the μ-analysis demonstrate that a VSM working as a virtual compensator shows higher robustness with respect to the VSG mode operation. Indeed, under the same nominal condition, the converter controlled as a VSC is stable for a larger range of uncertainty.

As a second contribution, this paper proposes for the first time in the literature a generic method to experimentally validate the μ-analysis outcomes. This approach is applied to experimentally demonstrate the theoretical results of the μ-analysis applied to the S-VSC model. The experimental results highlight the advantage of working as a VSC instead of a VSG from the robustness point of view.

This paper is organized as follows. Section II briefly describes the main blocks of the S-VSC structure and the difference between a virtual synchronous compensator and a virtual synchronous generator. Section III provides a theoretical description of the μ-analysis. Moreover, the analysis is applied to the S-VSC both for a simplified case and for a more general case. Next, in Section IV experimental tests validate the robust stability analysis and the higher robustness of the VSC mode operation over the VSG one. Finally, Section V concludes the paper.

II. Simplified Virtual Synchronous Compensator

The S-VSC is a voltage-input, current-output VSM [10], whose model is detailed in Fig. 2. All the quantities are expressed in per unit (pu), referred to the base values listed in Table I and Table II. The S-VSC consists of three main blocks:

- *Mechanical Emulation*: This block embeds the virtual swing equation by providing the virtual speed ω_r and the virtual angle θ_r from the virtual active power reference P_v^* and the virtual active power P_v;
- *Excitation Control*: it calculates the virtual excitation flux λ_e from the virtual reactive power reference Q_v^* and the virtual reactive power Q_v;
- *Electrical Equations*: this block implements the virtual stator equations. It receives as input θ_r, ω_r, the measured voltage v_g and λ_e. Its output is the virtual current i_v, used to calculate P_v and Q_v.

A detailed description of each block can be found in [10]. Assuming the S-VSC as a black box (highlighted in blue in Fig. 2) the inputs are P_v^*, Q_v^* and v_g. The output is the virtual current i_v. Next, the virtual current is added to the current reference i_i^* to retrieve the total current reference i^*. The current reference i_i^* is obtained from the inverter references P_i^* and Q_i^* through the *Power to Current* block. Therefore, there are two kinds of power references: the virtual power references P_v^* and Q_v^* and the inverter power references P_i^* and Q_i^*. The setpoints of power generation are indicated as P^* and Q^*.

If the S-VSC operates as a compensator (VSC mode), the virtual power references P_v^* and Q_v^* are always set to zero. In this way, the virtual part of the control algorithm is in charge only of the provision of the grid services, leaving the setpoints of power generation P^* and Q^* to the classical inverter structure (i.e., $P_i^* = P^*$, $Q_i^* = Q^*$) [10]. This is the main peculiarity of the S-VSC compared to the other solutions available in the literature, where the VSMs work as a VSG. Fig. 3 shows the control scheme of the S-VSC operating as a virtual compensator. The virtual current changes only during transients to provide grid services, such as inertial support. In steady-state, it is equal to zero. In this way, the power generation is linked to the fast dynamic of the current control loop (hundreds of Hz).

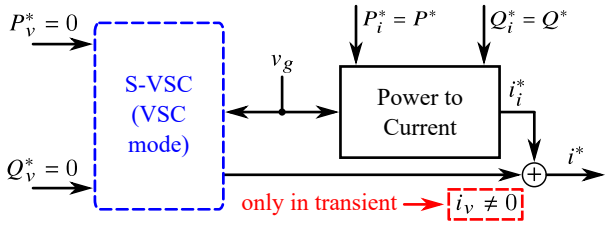

Fig. 3. Scheme of S-VSC model operating in VSC mode.

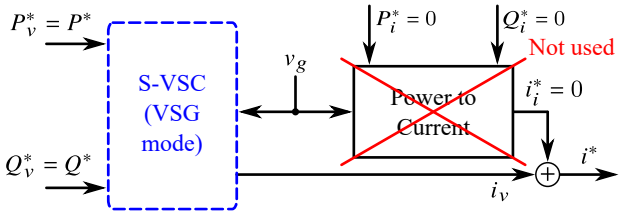

Fig. 4. Scheme of S-VSC model operating in VSG mode.

If the S-VSC operates as a generator (VSG mode), the virtual part is in charge of processing the full power references (i.e., $P_v^* = P^*$, $Q_v^* = Q^*$). Therefore, the *Power to Current* block is not used and i_v is equal to i^*, as depicted in Fig. 4. This is the typical behavior of the majority of the VSM solutions available in the literature. In this case, the power generation follows the slower dynamic of the virtual machine (several Hz), slowing down the response of the grid-connected converter to the variations of the power references P^*, Q^* [10].

III. Robust Stability Analysis

A. System under analysis

The goal of the μ-analysis is to validate the stability of a set of systems that differ from a system considered as reference (or rated), due to given uncertainties. The first step to perform the analysis consists of creating a model of the system shown in Fig. 1. In this paper, the system model is a state-space model in the Laplace domain linearized around a specific operating point (e.g., the nominal working point). The model is written in pu values referred to the base values reported in Table I and II. The schematic block of the system, illustrated in Fig. 5, consists of the following subsystems expressed in the (d,q) reference frame rotating at ω_r:

- *Controller C* is the state-space model of the inverter that is controlled according to the S-VSC control algorithm. The model is obtained by combining all the blocks depicted in Fig. 2. The block *C* has the following inputs and outputs:

$$\mathbf{u_C} = \left[\Delta i_{id}, \Delta i_{iq}, \Delta v_{gd}, \Delta v_{gq}, \Delta P^*, \Delta Q^*, \Delta\omega_g\right]^{\mathrm{T}} \quad (1)$$

$$\mathbf{y_C} = \left[\Delta e_{id}, \Delta e_{iq}, \Delta\omega_r\right]^{\mathrm{T}} \quad (2)$$

  where i_i is the inverter current, e_i is the inverter output voltage (assumed equal to the voltage reference v^* for the modeling), while ω_g is the grid frequency.
  The detailed state-space model can be retrieved from [11];

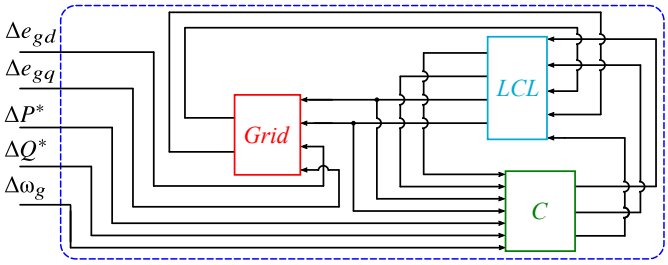

Fig. 5. Block scheme of the nominal system under study.

- *LCL* is the state-space model of the LCL filter, with the following inputs and outputs:

$$\mathbf{u_{LCL}} = \left[\Delta e_{id}, \Delta e_{iq}, \Delta i_{gd}, \Delta i_{gq}, \Delta\omega_r\right]^{\mathrm{T}} \quad (3)$$

$$\mathbf{y_{LCL}} = \left[\Delta i_{id}, \Delta i_{iq}, \Delta v_{gd}, \Delta v_{gq}\right]^{\mathrm{T}} \quad (4)$$

  where i_g is the grid current.
  The detailed state-space model can be retrieved from [11];
- *Grid* is the state-space model of the grid. The grid is modeled as a grid admittance. For this subsystem, the detailed state-space model is reported here:

$$\begin{cases} \dfrac{d\mathbf{x_{Grid}}}{dt} = \mathbf{A_{Grid}}\mathbf{x_{Grid}} + \mathbf{B_{Grid}}\mathbf{u_{Grid}} \\ \mathbf{y_{Grid}} = \mathbf{C_{Grid}}\mathbf{x_{Grid}} + \mathbf{D_{Grid}}\mathbf{u_{Grid}} \end{cases} \quad (5)$$

$$\mathbf{x_{Grid}} = \left[\Delta i_{gd}, \Delta i_{gq}\right]^{\mathrm{T}} \quad (6)$$

$$\mathbf{u_{Grid}} = \left[\Delta v_{gd}, \Delta v_{gq}, \Delta e_{gd}, \Delta e_{gq}\right]^{\mathrm{T}} \quad (7)$$

$$\mathbf{y_{Grid}} = \left[\Delta i_{gd}, \Delta i_{gq}\right]^{\mathrm{T}} \quad (8)$$

$$\mathbf{A_{Grid}} = \omega_b \begin{bmatrix} -\dfrac{R_g}{L_g} & \omega_{ro} \\ -\omega_{ro} & -\dfrac{R_g}{L_g} \end{bmatrix} ; \ \mathbf{C_{Grid}} = \mathbf{I}^{2x2} \quad (9)$$

$$\mathbf{B_{Grid}} = \frac{\omega_b}{L_g}\begin{bmatrix} 1 & 0 & -1 & 0 \\ 0 & 1 & 0 & -1 \end{bmatrix} ; \ \mathbf{D_{Grid}} = [\mathbf{0}]^{2x4} \quad (10)$$

  where e_g is the grid voltage, L_g is the grid inductance, R_g is the grid resistance and ω_{ro} is the value of the virtual speed at the linearized working point.

The overall state-space model of the system under study can be finally retrieved by applying the Component Connection Method (CCM) [12]–[14]. This is a widely-adopted solution available in the literature which consists of merging the state-space models of each subsystem into the overall state-space representation of the entire system in a modular manner.

B. Nominal Plant and Uncertainty Function

The second step is to identify a nominal plant $\mathbf{P_n}$ and a set of uncertain plants $\mathbf{\Pi_u}$. The uncertainty of a system can be modeled in several ways (e.g., parametric, additive, multiplicative) [15], [16]. In this paper, the uncertainty is multiplicative as follows [8]:

$$\mathbf{\Pi_u} = (\mathbf{I} + \mathbf{W})\mathbf{P_n} \quad (11)$$

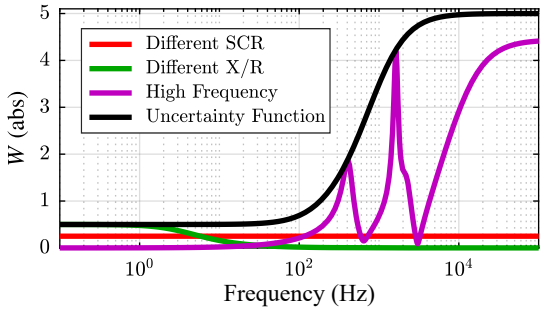

Fig. 6. Bode diagram of the uncertainty function W_u and its components.

where $\mathbf{I}$ is the identity matrix, $\mathbf{W}$ is a frequency-dependent uncertainty matrix and $\mathbf{\Pi_u}$ is a set of plants which differ from the nominal one for the given uncertainty $\mathbf{W}$.

The nominal plant $\mathbf{P_n}$ chosen for the analysis is the grid modeled by (5). Therefore, by considering the scheme of Fig. 5, the *Grid* block presents a certain degree of uncertainty, whereas both the Controller (block C) and the LCL filter (block *LCL*) are known, i.e., they are not affected by any uncertainty. For grid-connected converters, typical elements of uncertainty are the estimation of the grid impedance, grid reconfigurations and the effect of neighboring converters. Consequently, the uncertainty function W_u is built by considering the following uncertainties: 20% in the Short Circuit Ratio (SCR), 33% in the ratio between the grid reactance and resistance (i.e., X/R ratio) and additional resonant high-frequency effects as in [9]. The uncertainty matrix $\mathbf{W}$ can be finally built as follows:

$$\mathbf{W} = \begin{bmatrix} W_d & 0 \\ 0 & W_q \end{bmatrix} \tag{12}$$

where W_d and W_q are the uncertainty functions for the d-axis and q-axis, respectively. Moreover, $W_d = W_q = W_u$. Fig. 6 shows the Bode diagram of the uncertainty function W_u together with its components. The uncertainty function is obtained as an envelope of the single contributions [9]. The uncertain plants belonging to Π_p are obtained through all the uncertainties subtended by W_u.

C. Perturbation Matrix and MΔ structure

The third step of the μ-analysis is defining a set of perturbed uncertain plants $\mathbf{\Pi_p}$ as follows:

$$\mathbf{\Pi_p} = (\mathbf{I} + \mathbf{W\Delta})\mathbf{P_n} \tag{13}$$

where $\mathbf{\Delta}$ is the perturbation matrix.

The perturbation matrix $\mathbf{\Delta}$ is the unknown quantity and therefore represents the result of the μ-analysis. A priori, it is a generic matrix, which can be real or complex, diagonal or full, structured or unstructured [15], [16]. Finally, the final state-space model of the system can be built by adding the uncertainty block W and the perturbation block Δ into the scheme of Fig. 5 to obtain the final scheme illustrated in Fig. 7. The uncertainty block contains the uncertainty matrix $\mathbf{W}$, whereas the perturbation block contains the perturbation matrix $\mathbf{\Delta}$. A more compact representation of the block scheme is proposed in Fig. 8a, where G is the generalized plant obtained through the CCM. The structure of Fig. 8a is called $CG\Delta$ structure. For the fourth and final step, the $CG\Delta$ structure is reduced to the $N\Delta$ structure shown in Fig. 8b, through the linear fractional transformation (LFT) [15], [16]. Finally, the $M\Delta$ structure of Fig. 8c is obtained by considering only the inputs and outputs of M related to Δ. The $M\Delta$ structure is the system suitable to apply the μ-analysis.

D. Theory of the μ-analysis

In control theory, the structured singular value (denoted as SSV, or μ, here) is a mathematical concept that is defined to get necessary and sufficient conditions for robust stability [16]. The definition of μ is strictly related to the theorem described below [16]:

Theorem 1 (Determinant stability condition): Assume that the nominal system $\mathbf{M}(s)$ and the perturbations $\mathbf{\Delta}(s)$ are stable. [...] Then, the $M\Delta$ structure of Fig. 8c is stable for all allowed perturbations (we have robust stability) if and only if

$$\det[\mathbf{I} - \mathbf{M\Delta}(j\omega)] \neq 0 \ , \forall \omega, \forall \mathbf{\Delta} \text{ such that } ||\mathbf{\Delta}||_\infty \leq 1 \tag{14}$$

The complete theorem and its proof can be found in [16]. In (14), $||\mathbf{\Delta}||_\infty$ is the H_∞ norm of $\mathbf{\Delta}$. Starting from (14), the μ-analysis consists in finding, at each frequency ω, the smallest matrix $\mathbf{\Delta_{min}}$ (i.e., $\mathbf{\Delta}$ with the smallest maximum singular value $\overline{\sigma}$) which makes the matrix $\mathbf{I} - \mathbf{M\Delta}(j\omega)$ singular (i.e., makes its determinant equal to zero). The maximum singular value $\overline{\sigma}$ is equal to $||\mathbf{\Delta}||_\infty$. Then, μ is defined as the inverse of $\overline{\sigma}$. Mathematically, it results to:

$$\mu(\mathbf{M}) \triangleq \frac{1}{\min\limits_{\mathbf{\Delta}} \{\overline{\sigma}(\mathbf{\Delta}) \mid \det(\mathbf{I} - \mathbf{M\Delta}) = 0\}} \tag{15}$$

where μ is defined as $\mu = 1/\overline{\sigma}(\mathbf{\Delta})$ at each frequency.

Equation (15) is strictly valid for structured $\mathbf{\Delta}$ (not full matrix). However, (15) can be extended to the general unstructured case (full matrix) as demonstrated in [16]. Finally, the perturbation matrix $\mathbf{\Delta}$ is normalized such that $\overline{\sigma}(\mathbf{\Delta}) \leq 1$.

By applying the μ-analysis, it results that:

- At each frequency value, the determinant of (15) may be null for different values of $\mathbf{\Delta}$. Among all the possible solutions, the robust stability condition is satisfied by choosing the smallest matrix $\mathbf{\Delta_{min}}$. Such matrix identifies, at each frequency, the minimum condition to make the system unstable (measured in terms of the amplitude of its maximum singular value $\overline{\sigma}$);
- Since (15) is calculated at each frequency value in the considered range, $\mathbf{\Delta_{min}}$ is a function of the frequency as well. Among all the $\mathbf{\Delta_{min}}$ matrices calculated at each frequency ω_h, there is a value of frequency ω_k such that:

$$\begin{cases} ||\mathbf{\Delta_{min}}(j\omega_k)||_\infty < ||\mathbf{\Delta_{min}}(j\omega_h)||_\infty \ , \ \forall\ h \neq k \\ \mathbf{\Delta_{min}}(j\omega_k) = \mathbf{\Delta_{Min}} \\ \mu_{max} = \mu(\omega_k) = 1/\overline{\sigma}(\mathbf{\Delta_{Min}}) \end{cases} \tag{16}$$

According to (16), $\mathbf{\Delta_{Min}}$ is the smallest perturbation matrix along the entire range of frequency and μ_{max} is

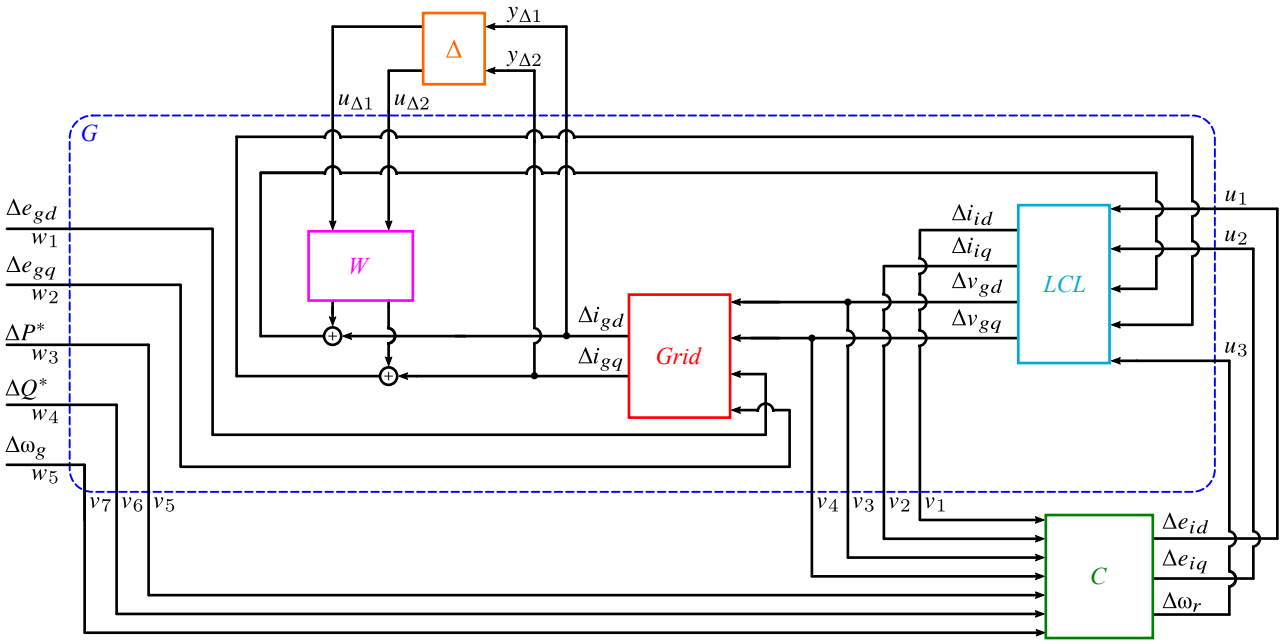

Fig. 7. Complete block scheme of the overall system to perform the μ-analysis.

the peak of μ along the entire range of frequency, both calculated at the frequency ω_k. Therefore, the minimum perturbation to make the system unstable is $\mathbf{\Delta_{Min}}$. Indeed, according to (15), there no exist a smaller matrix $\mathbf{\Delta}$ which nulls the determinant (i.e., makes the system unstable). Moreover, the system will diverge at the frequency ω_k. Consequently, μ_{max} represents an index of robustness because it allows to identify:

- The minimum condition to make the system unstable. The condition is fulfilled by $\mathbf{\Delta_{Min}}$ for the specific frequency ω_k;
- The oscillation frequency of the smallest unstable system (i.e., ω_k);
- The set of perturbed stable plants within the given set of uncertainty.

- The set of stable perturbed plants $\mathbf{\Pi_{p,s}}$ is obtained for all the matrices $\mathbf{\Delta}$ such that $\overline{\sigma}(\mathbf{\Delta}) < 1/\mu_{max}$;
- The set of unstable perturbed plants $\mathbf{\Pi_{p,u}}$ is obtained for all the matrices $\mathbf{\Delta}$ such that $\overline{\sigma}(\mathbf{\Delta}) > 1/\mu_{max}$ and for which $\det(\mathbf{I} - \mathbf{M\Delta}) = 0$.

In conclusion, based on the value of μ_{max}, the following conditions apply:

- If $\mu_{max} = 1$, all the plants in the set of uncertainty $\mathbf{\Pi_u}$ are stable;
- If $\mu_{max} > 1$, not all the plants in the set of uncertainty $\mathbf{\Pi_u}$ are stable, but only the plants belonging to the set $\mathbf{\Pi_{p,s}}$. Therefore, the higher is μ_{max}, the smaller is the set of stable plants for the given uncertainties;
- If $\mu_{max} < 1$, all the plants in the set of uncertainty $\mathbf{\Pi_u}$ are stable. Moreover, even the perturbed plants for which $1 \leq \overline{\sigma}(\mathbf{\Delta}) \leq 1/\mu_{max}$ are stable.

Therefore, μ_{max} provides the information on how large is set of stable plants for the given uncertainty. Indeed, the lower

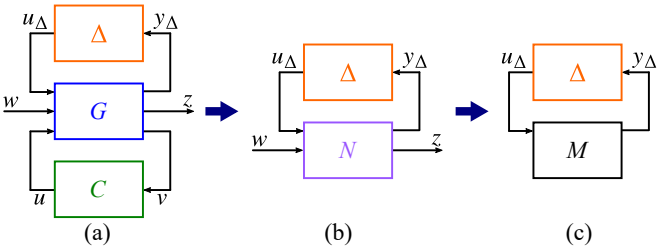

Fig. 8. Structure steps for the μ-analysis: (a) $CG\Delta$; (b) $N\Delta$; (c) $M\Delta$.

is μ_{max}, the larger is the set of stable plants. In other words, it quantifies the robustness of the system (i.e., the larger is the set of stable plants, more robust is the system).

E. Physical meaning of the μ-analysis

First, the μ-analysis is performed for a simplified case to clarify its physical meaning. For simplicity, the only element of uncertainty is the SCR. Considering an uncertainty of 20% in the SCR, the uncertainty matrix $\mathbf{W_{SCR}}$ can be written as follows:

$$\mathbf{W_{SCR}} = w_{SCR} \begin{bmatrix} 1 & 0 \\ 0 & 1 \end{bmatrix} = w_{SCR}\mathbf{I}^{2x2} \tag{17}$$

where $w_{SCR} = 0.25$ for the entire frequency range, as it can be observed in Fig. 6. Consequently, a set of uncertain plants can be defined as follows:

$$\mathbf{\Pi_{u,SCR}} = (\mathbf{I} + \mathbf{W_{SCR}})\mathbf{P_n} = (1 + w_{SCR})\mathbf{P_n} \tag{18}$$

Next, the set of perturbed uncertain plants is defined as follows:

$$\mathbf{\Pi_{p,SCR}} = (\mathbf{I} + \mathbf{W_{SCR}\Delta})\mathbf{P_n} \tag{19}$$

The μ-analysis is performed with the parameters listed in Table I and for an inverter active power injection of $P_i = 0.2$ pu. The parameters are the same as for the experimental setup.

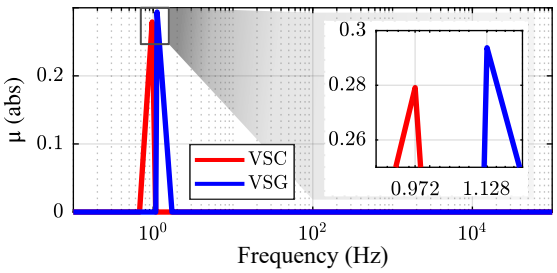

Fig. 9. μ-analysis of the S-VSC considering only the SCR as uncertainty: VSC operation in red, VSG operation in blue.

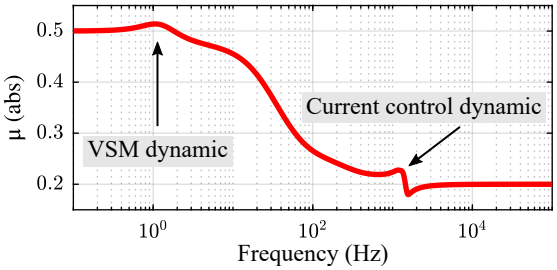

Fig. 10. μ-analysis result for the S-VSC with the uncertainty **W** operating as VSC.

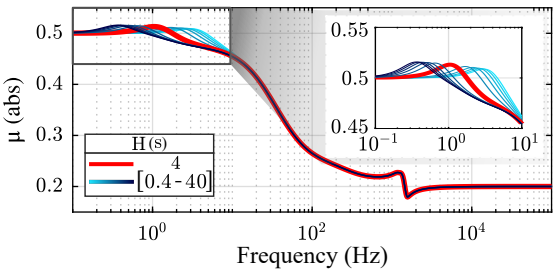

Fig. 11. μ-analysis result for the S-VSC with the uncertainty **W** operating as VSC for different values of the inertia constant H.

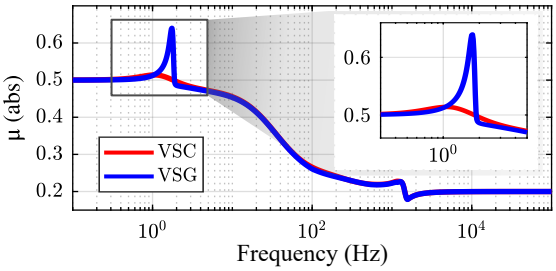

Fig. 12. μ-analysis result for the S-VSC with the uncertainty **W** operating as VSC (red) and VSG (blue).

The results for the S-VSC working both as VSC and VSG are proposed in Fig. 9. As it can be observed in Fig. 9, the analysis provides the value of μ in the considered frequency range. The μ-analysis identifies which are the stable plants belonging to the set of uncertain plants $\mathbf{\Pi_{u,SCR}}$. The minimum perturbed unstable plant $\mathbf{P_{p,u,min}}$ is obtained for the smallest perturbation matrix $\mathbf{\Delta_{Min}}$ which fulfills (15), as follows:

$$\mathbf{P_{p,u,min}} = (\mathbf{I} + \mathbf{W_{SCR}}\mathbf{\Delta_{Min}})\mathbf{P_n} = \frac{1}{k_{SCR}}\mathbf{I}^{2x2}\mathbf{P_n} \tag{20}$$

where:

$$\begin{cases} \mathbf{\Delta_{Min}} = k_\Delta \mathbf{I}^{2x2} \\ |k_\Delta| = ||\mathbf{\Delta_{Min}}||_\infty = 1/\mu_{max} \\ k_{SCR} = 1/(1 + w_{SCR} k_\Delta) \end{cases} \tag{21}$$

According to (20), the minimum condition to make the system unstable is matched for a grid impedance k_{SCR}-times the nominal one. The set of stable perturbed plants can be written as follows:

$$\mathbf{\Pi_{p,s,SCR}} = (\mathbf{I} + \mathbf{W_{SCR}}\mathbf{\Delta_s})\mathbf{P_n} = \frac{1}{k_{SCR,s}}\mathbf{I}^{2x2}\mathbf{P_n} \tag{22}$$

where:

$$\begin{cases} \mathbf{\Delta_s} = k_{\Delta,s}\mathbf{I}^{2x2} \\ |k_{\Delta,s}| = ||\mathbf{\Delta_s}||_\infty < ||\mathbf{\Delta_{Min}}||_\infty = |k_\Delta| \\ k_{SCR,s} = 1/(1 + w_{SCR} k_{\Delta,s}) < k_{SCR} \end{cases} \tag{23}$$

According to (22) and (23), the systems for which the grid impedance is lower than k_{SCR}-times the nominal value are stable. For the VSC mode, μ_{max} is equal to 0.278 at a frequency of 0.972 Hz and $\mathbf{\Delta_{Min}}$ is $-3.6 \cdot \mathbf{I}^{2x2}$. Consequently, k_{SCR} is equal to 10. This means that the minimum condition to make the system unstable is to increase the grid impedance by 10 times. In this limit case, the system will diverge with an oscillation frequency of 0.972 Hz. Similarly, for the VSG mode, μ_{max} is 0.292 with an oscillation frequency of 1.128 Hz, $\mathbf{\Delta_{Min}}$ is $-3.43 \cdot \mathbf{I}^{2x2}$ and k_{SCR} is 7. Therefore, in the VSG mode operation, the system becomes unstable for a lower increase of the grid impedance. This theoretical result demonstrates the higher robustness of the VSC compared to the VSG because, starting from the same nominal conditions, the S-VSC in VSC mode is stable for a larger set of perturbed plants (i.e., plants with a grid impedance from 7 to 10 times the nominal value). This result is experimentally validated in Section IV.

F. Robust Stability Analysis of the S-VSC

In this subsection, the robust stability analysis of the S-VSC is performed by considering the uncertainty function depicted in Fig. 6. The parameters used for the analysis are listed in Table II. They have been chosen as representative parameters for a more generic case of a power plant connected to the grid through power electronic converters. In this case, the system is linearized around the nominal working point of the inverter (i.e., $P^* = 1$ pu). The result of the μ-analysis for the S-VSC in VSC mode operation is proposed in Fig. 10. At each frequency, the value of μ is related to a specific dynamic. For instance, the virtual electromagnetic dynamic of the S-VSC (i.e., power loops and virtual stator) influences the value of μ only at low frequency (i.e., range between 0.1 Hz to 10 Hz). To demonstrate this, the analysis is repeated for different values of the virtual inertia constant H. The results are illustrated in Fig. 11. It can be observed that μ changes only in the range of frequency related to the virtual electromagnetic dynamic (i.e., 0.1 Hz to 10 Hz). On the opposite, the value of μ at high frequency (100 Hz to 10 kHz) does not change as it is

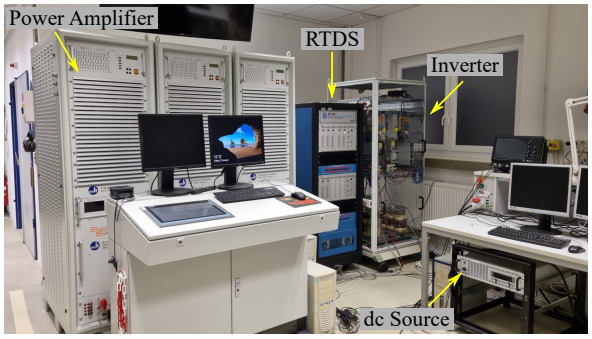

Fig. 13. Picture of the experimental setup.

TABLE I
EXPERIMENTAL SETUP PARAMETERS.

Inverter			**Base Values**		
S_N	4 kVA	S_b	4 kVA	ω_b	314 rad/s
I_N	10 A	V_b	$120\sqrt{2}$ V	L_b	34.4 mH
f_{sw}	10 kHz	Z_b	10.8 Ω	C_b	0.3 mF
VSM		**LCL Filter**		**Grid**	
R_v	0.02 pu	L_f	5 mH	$\widehat{E}_g$	$120\sqrt{2}$ V
L_v	0.2 pu	C_f	1.5 µF	L_g	2.5 mH
H	4 s	L_{fg}	0.5 mH	R_g	0.5 Ω

mostly dependent on the current dynamic (i.e., current control and LCL filter dynamic).

Next, the µ-analysis is performed for the VSG mode operation. The results for the VSC and the VSG mode operations are compared in Fig. 12. It can be noted that in the VSG mode operation, the peak of µ at low frequency is higher than the VSC case, whereas in the high frequency range the behavior of the two modes is almost the same. Therefore, the difference between the VSC and VSG mode operation influences only the response to low-frequency phenomena. It can be concluded that even in this general case, the S-VSC is more robust when operating as a virtual compensator because $\mu_{max,VSC} < \mu_{max,VSG}$ (i.e., $0.514 < 0.640$). Indeed, under the same conditions, the converter controlled as a compensator is stable for a larger number of perturbed plants (or, equivalently, for a larger set of uncertainty).

IV. EXPERIMENTAL VALIDATION

The experimental setup consists of a three-phase, two-level inverter connected to a power amplifier through an LCL filter. The power amplifier controlled by a Real-Time Digital Simulator (RTDS) emulates the grid. Fig. 13 illustrates a picture of the setup, while its main data are collected in Table I. Two kinds of experimental tests are performed to validate the theoretical results of the µ-analysis. As a first test, the state-space (S-S) models used to perform the µ-analysis have been validated through power references step variations.

Fig. 14a and Fig. 14b show the responses to the active power reference step of the S-VSC working as VSC and VSG, respectively. Both figures display the inverter active power P_i, the virtual active power P_v and the virtual frequency f. Fig. 14c illustrates the response to the virtual reactive power reference step, showing the inverter reactive power Q_i, the virtual reactive power Q_v and P_i. In all cases, the responses of the state-space models match the simulations and the experimental results, thus demonstrating the validity of the modeling procedure. The uncertainty function used to perform the µ-analysis of subsection III-F replicates a general case taking into account several sources of uncertainty. However, it is not possible to experimentally validate such a general case. For this reason, the outcome of the µ-analysis has been validated for the simplified case described in subsection III-E. As already stated in the previous section, an uncertainty only on the SCR is equivalent to a variation of the grid impedance.

TABLE II
SIMULATION PARAMETERS.

Inverter		**Base Values**			
S_N	100 kVA	S_b	100 kVA	ω_b	314 rad/s
I_N	205 A	V_b	$230\sqrt{2}$ V	L_b	5.1 mH
f_{sw}	10 kHz	Z_b	1.6 Ω	C_b	2 mF
VSM		**LCL Filter**		**Grid**	
R_v	0.02 pu	L_f	0.05 pu	$\widehat{E}_g$	$230\sqrt{2}$ V
L_v	0.2 pu	C_f	0.05 pu	L_g	0.02 pu
H	4 s	L_{fg}	0.08 pu	R_g	0.002 pu

The first test consists of using a grid impedance 7 times higher than the nominal one and applying an active power reference step from 0 pu to 0.2 pu. The experimental result for the VSG mode operation is proposed in Fig. 15a. It can be observed that working as VSG, the S-VSC diverges at 1.101 Hz, matching the theoretical results. Under the same conditions, the S-VSC operating as VSC slowly converges as illustrated in Fig. 15b, demonstrating the higher robustness of the virtual compensator operation. Finally, the grid impedance is increased by 10 times. The VSC slowly diverges at a frequency of about 0.989 Hz, validating the theoretical outcomes of the µ-analysis as demonstrated in Fig. 15c.

V. CONCLUSION

Plant uncertainties (e.g., wrong grid impedance estimation), grid reconfigurations and the influence of neighboring converters might affect the stability of grid-connected converters. The µ-analysis is a valuable method to evaluate the robust stability of grid-connected converters for a given set of uncertainty. In the literature, this method has been applied to converters behaving as VSGs to support the grid by providing ancillary services. However, the differences in terms of robustness between a VSC and a VSG have never been investigated in the literature. Therefore, as a first contribution, this paper proposed the robust stability analysis of a VSM working both as a virtual compensator and generator. The theoretical analysis demonstrated that a VSM working as a virtual compensator shows higher robustness with respect to the VSG mode operation. Indeed, under the same nominal condition, the VSC operation is stable for a larger set of uncertain plants. Moreover, the µ-analysis outcomes have never been experimentally validated in the literature so far. Therefore, as a second contribution, this paper provided the experimental validation of the µ-analysis applied to the S-VSC control algorithm. In conclusion, the theoretical analysis, validated by

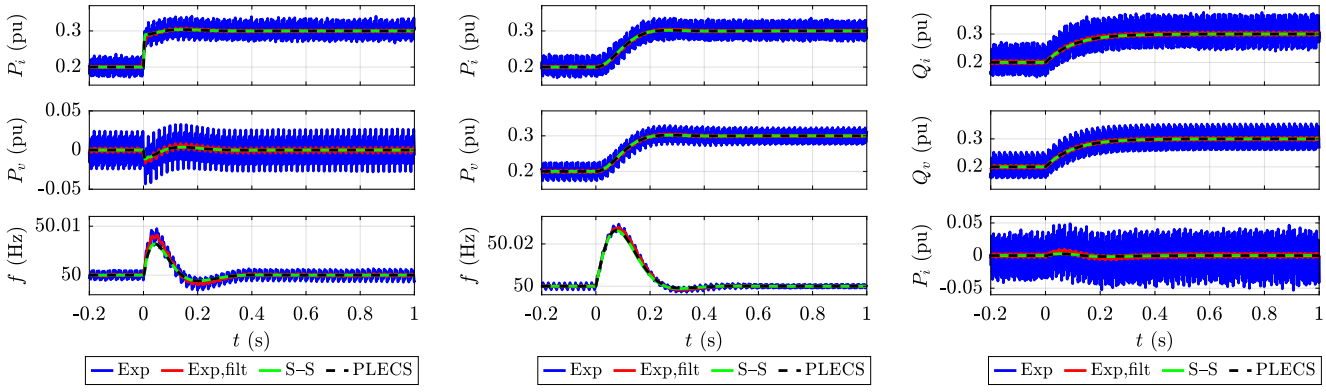

(a) (b) (c)

Fig. 14. (a) Active power reference step response in VSC mode; (b) Active power reference step response in VSG mode; (c) Reactive power reference step response in VSG mode.

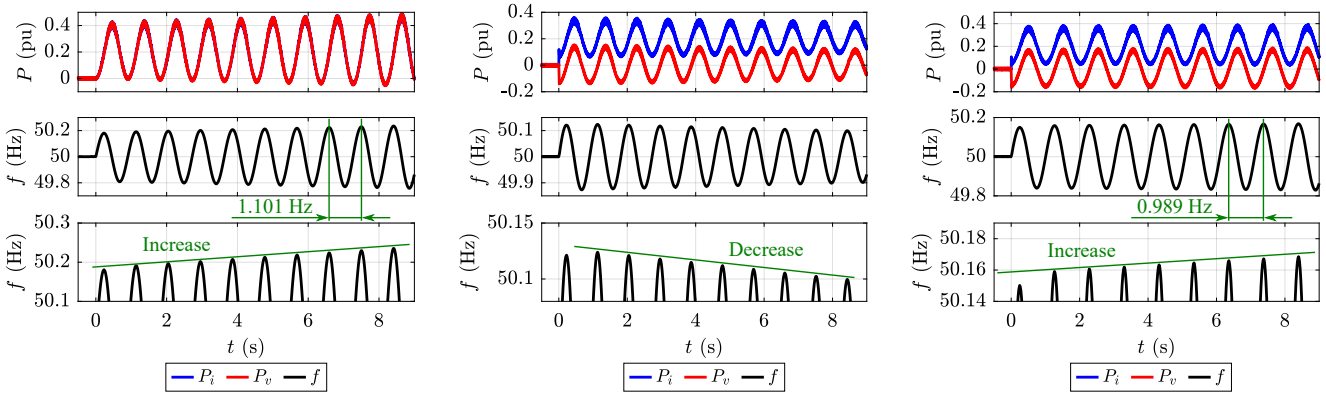

(a) (b) (c)

Fig. 15. Instability tests in: (a) VSG mode with k_{SCR} = 7; (b) VSC mode with k_{SCR} = 7; (c) VSC mode with k_{SCR} = 10.

experimental results, highlights the advantage of working as a virtual compensator instead of a virtual generator from the robustness point of view.

REFERENCES

[1] ENTSO-E, "High Penetration of Power Electronic Interfaced Power Sources and the Potential Contribution of Grid Forming Converters," Jan. 2020, Technical Report.

[2] nationalgridESO, "GC0137: Minimum Specification Required for Provision of GB Grid Forming (GBGF) Capability (formerly Virtual Synchronous Machine/VSM Capability)," Mar. 2021, Technical Report.

[3] ENTSO-E, "Frequency Stability in Long-Term Scenarios and Relevant Requirements," Dec. 2021, Technical Report.

[4] Terna, "Code for Transmission, Dispatching, Development and Security of the Grid," Mar. 2023, Grid Code.

[5] M. Chen, D. Zhou, and F. Blaabjerg, "Modelling, Implementation, and Assessment of Virtual Synchronous Generator in Power Systems," *Journal of Modern Power Systems and Clean Energy*, vol. 8, no. 3, pp. 399–411, May 2020.

[6] V. Mallemaci, F. Mandrile, S. Rubino, A. Mazza, E. Carpaneto, and R. Bojoi, "A comprehensive comparison of Virtual Synchronous Generators with focus on virtual inertia and frequency regulation," *Electric Power Systems Research*, vol. 201, p. 107516, Dec. 2021.

[7] M. Shadoul, R. Ahshan, R. S. AlAbri, A. Al-Badi, M. Albadi, and M. Jamil, "A comprehensive review on a virtual-synchronous generator: Topologies, control orders and techniques, energy storages, and applications," *Energies*, vol. 15, no. 22, 2022.

[8] R. Rosso, J. Cassoli, G. Buticchi, S. Engelken, and M. Liserre, "Robust Stability Analysis of LCL Filter Based Synchronverter Under Different Grid Conditions," *IEEE Transactions on Power Electronics*, vol. 34, no. 6, pp. 5842–5853, Jun. 2019.

[9] R. Rosso, S. Engelken, and M. Liserre, "Robust Stability Investigation of the Interactions Among Grid-Forming and Grid-Following Converters," *IEEE Journal of Emerging and Selected Topics in Power Electronics*, vol. 8, no. 2, pp. 991–1003, Jun. 2020.

[10] F. Mandrile, E. Carpaneto, and R. Bojoi, "Grid-Feeding Inverter With Simplified Virtual Synchronous Compensator Providing Grid Services and Grid Support," *IEEE Transactions on Industry Applications*, vol. 57, no. 1, pp. 559–569, Jan. 2021.

[11] V. Mallemaci, F. Mandrile, E. Carpaneto, and R. Bojoi, "Simplified virtual synchronous compensator with grid–forming capability," *IEEE Transactions on Industry Applications*, pp. 1–17, 2023, Early Access.

[12] Y. Wang, X. Wang, Z. Chen, and F. Blaabjerg, "Small-signal stability analysis of inverter-fed power systems using component connection method," *IEEE Transactions on Smart Grid*, vol. 9, no. 5, pp. 5301–5310, 2018.

[13] F. Mandrile, S. Musumeci, E. Carpaneto, R. Bojoi, T. Dragičević, and F. Blaabjerg, "State-space modeling techniques of emerging grid-connected converters," *Energies*, vol. 13, no. 18, 2020.

[14] R. Rosso, S. Engelken, and M. Liserre, "Robust stability analysis of synchronverters operating in parallel," *IEEE Transactions on Power Electronics*, vol. 34, no. 11, pp. 11 309–11 319, 2019.

[15] K. Zhou and J. C. Doyle, *Essentials of robust control*. Prentice Hall, 1998.

[16] S. Skogestad and I. Postlethwaite, *Multivariable Feedback Control: Analysis and Design*. John Wiley and Sons, 2001.